Mechatronics 107 (2025) 103306

Contents lists available at ScienceDirect

Mechatronics

journal homepage: www.elsevier.com/locate/mechatronics

Parametric design of PI controllers for piezoelectric ultrasonic transducers ☆

Diego Stutzer [a,d], André Lisibach [b], Martin Hofmann [c], Jürgen Burger [c], Thomas Niederhauser [a,*]

[a] Institute for Human Centered Engineering HuCE, Bern University of Applied Sciences, Biel, Switzerland
[b] Institute for Optimisation and Data Analysis IODA, Bern University of Applied Sciences, Biel, Switzerland
[c] School of Biomedical and Precision Engineering, University of Bern, Bern, Switzerland
[d] Graduate School for Cellular and Biomedical Sciences, University of Bern, Bern, Switzerland

ARTICLE INFO

Keywords:
Piezoelectric ultrasonic transducer
Proportional–integral
Feedback controller
Pole-zero cancellation
Periodontal scaler

ABSTRACT

Piezoelectric ultrasonic transducers are widely used and can offer great benefits, e.g., in ultrasonic machining, cleaning, and cutting. However, due to the resonance behavior of these transducers, feedback controllers that track the resonance frequency and regulate the vibration amplitude are often indispensable to ensure efficiency. This article presents a generic and efficient approach to designing proportional–integral controllers for piezoelectric ultrasonic transducers using the method of pole-zero cancellation based on a model of their vibration amplitude and phase dynamics. The parametric design method was experimentally applied to a piezoelectric ultrasonic periodontal scaler and compared with other tuning methods to demonstrate its advantages. The parametric design methodrequired ten times fewer experiments to parameterize the controller than the Ziegler–Nichols method, for instance, and resulted in a closed-loop system with better load rejection than the other tuning methods. The results document that the new method can considerably simplify and accelerate the development of performant feedback controllers for piezoelectric ultrasonic transducers.

1. Introduction

Piezoelectric ultrasonic transducers (PUTs) are used in various industrial and clinical applications such as ultrasonic machining, cleaning, and cutting. As the electro-mechanical bandwidth of PUTs is typically very narrow, they must be operated precisely at their resonance frequency to generate sufficient vibration. However, PUTs often manifest considerable variations during operation, e.g., changes in the resonance frequency and the vibration amplitude due to varying load, self-heating, or aging [1–5].

Consequently, PUTs require feedback controllers that track the resonance frequency and maintain a constant vibration amplitude in most applications. Although sophisticated control algorithms have gained attention in the scientific community [6–11], proportional (P), proportional–integral (PI), and proportional–integral–differential (PID) controllers are still widely used not only in industrial systems but also in research applications. Such controllers are highly popular as they can deliver excellent performance, while their simple structure and low complexity enable rapid implementation at low cost.

The design of such controllers typically relies on empirical tuning [12–17] or heuristic methods [18–22]. Empirical tuning involves time-consuming repetitions of parameter adjustments and experiments to analyze the resulting controller performance by trial and error. The results largely depend on the engineer's expertise and effort and may be limited to specific transducers. Similarly, heuristic approaches, such as the Ziegler–Nichols method [23], typically require numerous and potentially destructive experiments, e.g., to search for the ultimate gain at which the control loop's output manifests sustained and stable oscillations. Furthermore, they may lack the potential to achieve specific design targets such as desired closed-loop response times.

Apart from these two concepts, various other methods to tune PI controllers are described in scientific literature, e.g., the modified Ziegler–Nichols (MZN) method [24], the Tyreus-Luyben (TL) method [25], Kappa-Tau (KT) tuning [24], or internal model control (IMC) [26]. Even though these methods are not common to tune controllers for PUTs, they may also offer some benefits in this application as well since they result in a closed-loop system with better damping and higher robustness.

In contrast to the aforementioned concepts, I. Ille et al. proposed an approach to parameterize PI controllers for PUTs based on a model of the amplitude and phase dynamics derived from the Butterworth–Van

☆ This paper was recommended for publication by Associate Editor Minghui Zheng.

* Corresponding author.
E-mail address: thomas.niederhauser@bfh.ch (T. Niederhauser).

https://doi.org/10.1016/j.mechatronics.2025.103306
Received 3 May 2024; Received in revised form 13 February 2025; Accepted 13 February 2025
Available online 27 February 2025

Dyke (BVD) [27]. However, the article does not outline the procedure in detail, and we empirically found that the model's accuracy is limited during fast transients of the driving voltage amplitude and frequency [6].

In previous work, our group investigated the operation of piezoelectric ultrasonic periodontal scalers (PUPS) based on PUTs in a conventional Langevin configuration and based on planar PUTs [1,28–30]. One study revealed that the force exerted by periodontists and dental hygienists on PUPS frequently varies considerably during use, which underlines the importance of a feedback control system [30]. The parameterization of proportional–integral–derivative (PID) controllers for these devices with empirical or heuristic methods was very time-consuming and the performance of the resulting closed-loop system was not allays satisfying. Based on our experience and since a derivative action of a feedback controller tends to amplify noise, we suspected that a proportional–integral (PI) controller could be expedient in the given application. Consequently, we developed a new method to parametrically design PI controllers for PUTs based on the method of pole-zero cancellation (PZC) [31,32]. By applying harmonic averaging to the BVD model, we derived a model that accurately reproduces the vibration amplitude and phase dynamics of PUTs, even during fast transients of the driving voltage amplitude and frequency [6]. This article outlines how this model can be used to design PI controllers for PUTs using PZC and presents the results of an experimental application to a piezoelectric ultrasonic periodontal scaler (PUPS) in comparison to other tuning methods. This article aims to provide scientists and engineers with a new method to design PI controllers for PUTs with excellent closed-loop behavior and minimal effort.

Section 2 presents essential materials and methods, including the model for the vibration amplitude and phase dynamics and the parametric method to design PI controllers for PUTs. Section 4 subsequently documents the results of an experimental application of the parametric design method and other tuning methods to control a PUPS. The results are discussed in Section 5, followed by Section 6, concluding this article.

2. Materials and methods

2.1. Piezoelectric ultrasonic periodontal scaler

The PUPS depicted in Fig. 1(a) was used to experimentally evaluate the parametric method to design PI controllers for PUTs outlined in Section 3. This PUPS is based on a Langevin-type PUT with a nominal resonance frequency of approximately 29.5 kHz and driven by a sinusoidal voltage with amplitudes up to 100 V.

2.2. Butterworth–Van Dyke model

The BVD model is an electrical equivalent circuit consisting of four parameters, namely C_0, C, L, and R, as depicted in Fig. 1(b), and is frequently used to model PUTs [33]. While C_0 represents the PUT's electrical capacitance, the series circuit comprising R, L, and C mimics the transducer's electro-mechanical coupling and oscillation. The velocity v of the PUT's mechanical oscillation is assumed to be proportional to the so-called mechanical current i_m through R, L, and C, by a coupling factor denoted by α hereafter, i.e., $v \approx \alpha\, i_m$. In the given application, the PUT is driven by a sinusoidal voltage $u(t)$ with an amplitude denoted by $\hat{u}(t)$ and an angular frequency denoted $\omega(t)$ hereafter, i.e.,

$$u(t) = \hat{u}(t)\, \sin(\omega(t)\, t). \tag{1}$$

Consequently, the PUT generates a mechanical oscillation with an approximately sinusoidal velocity $v(t)$ that can be described by

$$v(t) = \hat{v}(t)\, \sin(\omega(t)\, t + \phi(t)), \tag{2}$$

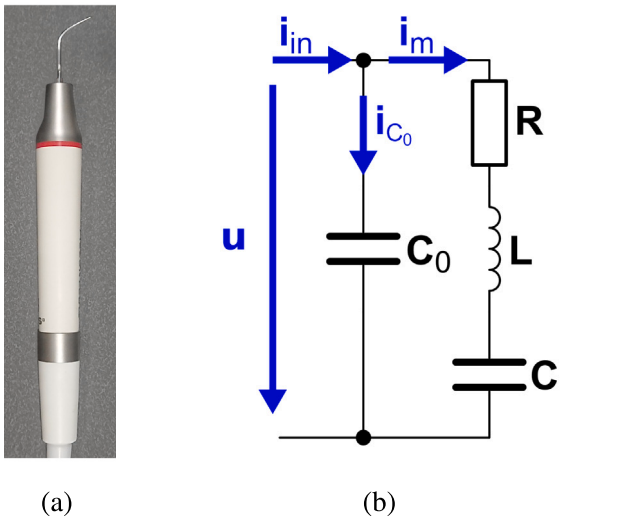

Fig. 1. (a) Piezoelectric ultrasonic periodontal scaler (PIEZON LED Handpiece, Electro Medical Systems SA, Nyon, Switzerland) used for the experimental verification. (b) Butterworth Van-Dyke model for piezoelectric ultrasonic transducers.

where $\hat{v}(t)$ denotes the velocity's amplitude and $\phi(t)$ its phase with respect to $u(t)$.

In the BVD model, the impedances of the static capacitance Z_{C_0}, of the mechanical branch Z_m, and at the input Z_{in}, in dependence of the angular frequency ω, are given by

$$Z_{C_0}(\omega) = \frac{1}{i\,\omega\, C_0}, \tag{3}$$

$$Z_m(\omega) = R + i\,\omega\, L + \frac{1}{i\,\omega\, C}, \quad \text{and} \tag{4}$$

$$Z_{in}(\omega) = \frac{Z_{C_0}(\omega)\, Z_m(\omega)}{Z_{C_0}(\omega) + Z_m(\omega)}, \tag{5}$$

where i denotes the imaginary unit.

As stated above, the PUT's vibration velocity v is proportional to the current through the mechanical branch and, thus, related to the driving voltage u and Z_m by

$$v(t) = \alpha\, \frac{u(t)}{Z_m(t)}. \tag{6}$$

This implies that the vibration velocity's amplitude $\hat{v}$ and phase ϕ can be described by

$$\hat{v}(t) = \alpha\, \frac{\hat{u}(t)}{|Z_m(t)|}, \quad \text{and} \tag{7}$$

$$\phi(t) = -\angle Z_m(t). \tag{8}$$

At resonance frequency ω_n, defined as

$$\omega_n = \frac{1}{\sqrt{L\, C}}, \tag{9}$$

the magnitude of Z_m is equal to R, and its phase is zero, i.e.,

$$Z_m(\omega_n) = R. \tag{10}$$

Consequently, the vibration velocity's phase ϕ is zero at the resonance frequency in this case. Furthermore, the vibration velocity's amplitude $\hat{v}$ is maximal in this case, since $|Z_m(w)| \geq R \;\forall\; \omega \neq \omega_n$.

At frequencies far away from resonance, the input impedance Z_{in} is dominated by the static capacitance C_0 and can be approximated by

$$Z_{in}(\omega) \approx \frac{1}{i\,\omega\, C_0}, \quad \text{if} \quad |\omega - \omega_n| \gg 0. \tag{11}$$

2.3. Amplitude and phase dynamics model

By applying harmonic averaging to the mechanical branch of the BVD model [6], we demonstrated that the small signal dynamics of the vibration velocity's amplitude and phase can be approximated with high accuracy by first-order linear time-invariant systems with time constants $\tau_{\hat{v}}$ and τ_{ϕ}, respectively, i.e., by the transfer functions

$$G_{p_{\hat{v}}}(s) = \frac{\hat{V}(s)}{\hat{U}(s)} \approx \frac{\alpha}{2\,L\,s + R} = \frac{\frac{\alpha}{2\,L}}{s + \frac{1}{\tau_{\hat{v}}}}, \quad \text{and} \tag{12}$$

$$G_{p_{\phi}}(s) = \frac{\Phi(s)}{\Delta\Omega(s)} \approx \frac{-2\,L}{2\,L\,s + R} = \frac{-1}{s + \frac{1}{\tau_{\phi}}}, \quad \text{with} \tag{13}$$

$$\tau_{\hat{v}} = \tau_{\phi} = \frac{2\,L}{R}, \tag{14}$$

if the PUT is operated near resonance and $C/L \approx 0$ holds. Here, $\hat{U}$, $\Delta\Omega$, $\hat{V}$, and Φ denote the Laplace transforms of $\hat{u}$, $\Delta\omega = \omega - \omega_n$, $\hat{v}$, and ϕ, respectively.

As outlined by other authors, the time constants also characterize the step response times, i.e., the time after which the vibration velocity's amplitude and phase reach $\sim 63\%$ of the step height after a change of the driving voltage amplitude and frequency, respectively [34].

In analogy to Eqs. (12) and (13), discretized transfer functions can be given by

$$G_{p_{\hat{v}}}(z) = \frac{\hat{V}(z)}{\hat{U}(z)} \approx \frac{-\frac{\alpha}{R}\,(e^{-\frac{R\,T_s}{2\,L}} - 1)}{z - e^{-\frac{R\,T_s}{2\,L}}} \quad \text{and} \tag{15}$$

$$G_{p_{\phi}}(z) = \frac{\Phi(z)}{\Delta\Omega(z)} \approx \frac{\frac{2\,L}{R}\,(e^{-\frac{R\,T_s}{2\,L}} - 1)}{z - e^{-\frac{R\,T_s}{2\,L}}}, \tag{16}$$

where T_s denotes the sampling period [34].

2.4. Control structure

Two PI controllers operating in parallel are used to track the resonance frequency and regulate the vibration amplitude of the PUT, as illustrated in Fig. 2. One PI controller regulates the vibration velocity amplitude $\hat{v}$ to a setpoint $\hat{v}_{set}$ by modifying the driving voltage amplitude $\hat{u}$ using the control law

$$G_{c_{\hat{v}}}(s) = \frac{\hat{U}(s)}{E_{\hat{v}}(s)} = K_{p_{\hat{v}}} + \frac{K_{i_{\hat{v}}}}{s}, \tag{17}$$

where the amplitude error $e_{\hat{v}}$ is given by

$$e_{\hat{v}} = \hat{v}_{set} - \hat{v}. \tag{18}$$

A second PI controller regulates the phase of the vibration velocity ϕ to $0°$ to track the resonance frequency by modifying the driving frequency ω using the control law

$$G_{c_{\phi}}(s) = \frac{\Delta\Omega(s)}{E_{\phi}(s)} = K_{p_{\phi}} + \frac{K_{i_{\phi}}}{s}, \tag{19}$$

where the phase error e_{ϕ} is given by

$$e_{\phi} = 0° - \phi. \tag{20}$$

Subsequently, a sinusoidal voltage is synthesized to drive the PUT, i.e.,

$$u = \hat{u}\,\sin((\omega_n + \Delta\omega)\,t). \tag{21}$$

For the implementation on digital control systems, discretized versions of these Equations may be required. In analogy to (17) and (19), the discrete-time control laws can be given by

$$G_{c_{\hat{v}}}(z) = \frac{\hat{U}(z)}{E_{\hat{v}}(z)} = K_{p_{\hat{v}}} + K_{i_{\hat{v}}}\,\frac{T_s}{z-1} \quad \text{and} \tag{22}$$

$$G_{c_{\phi}}(z) = \frac{\Delta\Omega(z)}{E_{\phi}(z)} = K_{p_{\phi}} + K_{i_{\phi}}\,\frac{T_s}{z-1}. \tag{23}$$

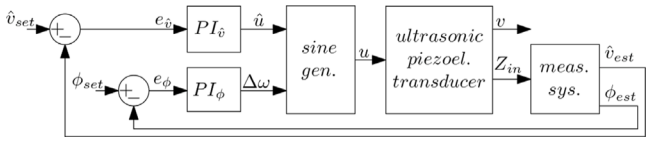

Fig. 2. Block diagram of control structure comprising a PI controller ($PI_{\hat{v}}$) to regulate the estimated vibration velocity amplitude, and a PI controller (PI_{ϕ}) to track the resonance frequency. The vibration velocity is estimated since its direct measurement is impaired in the given application.

Some PUTs, e.g., the PUPS described in Section 2.1, do not comprise a sensor to measure the vibration velocity v. In this case, the vibration velocity's amplitude $\hat{v}$ and phase ϕ can be estimated based on measurements of the input impedance Z_{in}, for instance by mathematically compensating the influence C_0 based on Eq. (5), i.e.,

$$Z_m = \frac{1}{\frac{1}{Z_{in}} - i\,\omega\,C_0}, \tag{24}$$

$$\hat{v}_{est} = \alpha\,\frac{\hat{u}}{|Z_m|}, \quad \text{and} \tag{25}$$

$$\phi_{est} = -\angle Z_m. \tag{26}$$

2.5. Electronic control system

A custom-built electronic system developed in previous work [35], based on a microcontroller development board (NUCLEO-H743ZI2, ST-Microelectronics, Geneva, Switzerland) and a power amplifier ("PX200-V100,100", PiezoDrive, Shortland, Australia) was used to implement the PI controllers.

The PUPS's driving voltage and input current are preconditioned by analog circuits and sampled by ADCs. These measurements are used to calculate updated values of the driving voltage amplitude $\hat{u}$ and frequency ω as outlined in Section 2.4. An updated sinusoidal signal is then generated by a DAC, amplified, and applied to the PUPS. The sampling period of the control system is fixed to $T_s = 0.5\,\text{ms}$. The driving voltage amplitude can vary from 1 V up to 100 V and the driving frequency from 20 kHz to 40 kHz.

2.6. Measurement setup

A custom-built measurement system developed in previous work [1], controlled by MATLAB (R2021a, The MathWorks Inc., Natick, Massachusetts, USA), was used to measure the vibration velocity at the tip of the PUPS using a laser Doppler vibrometer connected to a DAQ module and a computer. Additionally, the measurement system can apply a lateral force at the tip of the PUPS using a wet laboratory slab and measure it using a three-axis force sensor. To record the PUPS's driving voltage and input current, the electronic system outlined in Section 2.5 was used.

2.7. Simulation

The control system and the PUPS were simulated in MATLAB. The discrete-time control loop was simulated based on the equations in Section 2.4 complemented by code to simulate implementation-specific aspects of the electronic control system presented in Section 2.5. The PUPS was simulated using the BVD model outlined in Section 2.2 with the values listed in Table 1.

2.8. Conventional tuning methods

To evaluate the performance of the parametric design method presented in Section 3, it is compared to various tuning methods for PI controllers described in scientific literature.

2.8.1. Ziegler–Nichols (ZN) method

According to the ZN method [23], iterative experiments with a purely proportional controller are conducted in a first step. The gain is varied until the so-called ultimate gain K_u is found, at which the output of the closed-loop system exhibits a stable oscillation. The period of this stable oscillation T_u is then measured and used together with the ultimate gain to determine the gains for the controller based on empirically derived equations, i.e., $K_p = 0.45\,K_u$ and $K_i = 0.54\,\frac{K_u}{T_u}$ [23]. In the application for the PUPS, 11 and 16 experiments were required to determine K_u and T_u for the amplitude and phase controller, respectively.

2.8.2. Modified Ziegler–Nichols (MZN) method

The MZN method is similar to the ZN method but can result in a closed-loop system with improved damping [24]. As outlined by Astrom et al. the gains are calculated by $K_p = K_u\,r_b\cos(\phi_b)$ and $K_i = \frac{2\pi K_u r_b \sin(\phi_b)}{T_u}$ in this case, where a reasonable choice of the tuning parameters r_b and ϕ_b is 0.5 and 20°, respectively [24].

2.8.3. Tyreus-Luyben (TL) method

The method by Tyreus and Luyben (TL) is similar to the ZN method, too, aiming to improve the robustness and reduce oscillatory effects [25]. As for the ZN method, the controller gains are calculated based on a measurement of the ultimate gain K_u and the resulting oscillation period T_u. However, according to the TL method, the gains are calculated by $K_p = \frac{K_u}{3.2}$ and $K_i = \frac{K_p}{2.2\,T_u}$ for a PI controller.

2.8.4. Kappa-Tau (KT) method

The method of Kappa-Tau (KT) tuning comprises several variations and can be considered as a generalization of the ZN method, with which better damping and rejection of load disturbances can be achieved, as outlined by Astrom and Hägglund [24]. In contrast to other methods, the KT is based on a two-degree-of-freedom PI (or PID) controller, which includes a setpoint weighting on the proportional (and eventually on the derivative) term. Such a PI controller can be described by $u(s) = K_p\,(b\,y_{set} - y) + \frac{K_p}{T_i\,s}(y_{set} - y)$. In the application for the PUPS, we applied the tuning formulas based on the so-called frequency-response method [24]. As the ZN method, this requires knowledge of the ultimate gain K_u and of the oscillation period T_u. Additionally, knowledge of the plant's static gain K is required, and the tuning parameter maximum sensitivity M_s has to be selected, typically in the range from 1.4 to 2.0. On the PUPS, we tested amplitude- and phase-controllers based on this method with a maximum sensitivity of $M_s = 1.4$ (abbreviated as KT14) and $M_s = 2.0$ (KT20), respectively. Based on the gain ratio $\kappa = \frac{1}{K_u\,K}$, the controller parameters K_p, T_i, and b, are calculated as follows: For $M_s = 1.4$ they are calculated by $K_p = 0.053e^{2.9\kappa-2.6\kappa^2}K_u$, $T_i = 0.9e^{-4.4\kappa+2.7\kappa^2}T_u$, and $b = 1.1e^{-0.0061\kappa+1.8\kappa^2}$. For $M_s = 2.0$ they are calculated by $K_p = 0.13e^{1.9\kappa-1.3\kappa^2}K_u$, $T_i = 0.9e^{-4.4\kappa+2.7\kappa^2}T_u$, and $b = 0.48e^{-0.4\kappa-0.17\kappa^2}$.

2.8.5. Internal model control (IMC)

The method of IMC [26] assumes that the system to be controlled can be approximated by a first-order model without delay, i.e., by a transfer function of the form $G_p(s) = \frac{K}{\tau s+1}$. Based on this model and the chosen desired closed-loop response time τ_{CL} the gains of PI controllers are then calculated by $K_p = \frac{\tau}{K\tau_{CL}}$ and $K_i = \frac{\tau}{K\tau_{CL}\min(\tau,4\tau_{CL})}$. In the application for the PUPS, the parameters of the amplitude and phase dynamics models, as presented in Section 2.3, were identified from a frequency sweep, as outlined in Section 3.1. In this case, $\tau = \frac{2L}{R}$ for both controllers, while $K = \frac{\alpha}{R}$ for the amplitude controller and $K = \frac{-2L}{R}$ for the phase controller, as can be seen from Eqs. (12), (13), and (14).

Table 1
Model parameters of the piezoelectric ultrasonic periodontal scaler.

	Values without load applied at the tip	Values with ~0.25 N applied at the tip
C_0	1.6 nF	1.6 nF
R	194.3 Ω	238.9 Ω
L	828.2 mH	828.5 mH
C	35.1 pF	35.1 pF
α	39.5 m/(As)	39.5 m/(As)

3. Parametric design of PI controllers by pole-zero cancellation (PZC)

3.1. System identification

For the parametric design, illustrated in Fig. 3, the model parameters of the PUT have to be identified. The transfer functions in the Eqs. (12) and (13) allow to take the frequency and step responses into account for the calculation of these parameters.

First, the PUT's input impedance is measured during a frequency sweep, preferably at a driving voltage amplitude similar to that in the foreseen application. C_0 is then calculated using Eq. (11) from the value of Z_{in} at a frequency sufficiently far away from resonance. Subsequently, the values of Z_m are calculated using Eq. (24). The resonance frequency ω_n is then identified as the frequency where $\angle Z_m = 0$ and the value of $R = |Z_m(\omega_n)|$ is read out, as indicated in Eq. (10).

Second, the vibration velocity amplitude of the PUT during a step of the driving voltage amplitude at resonance frequency is measured. L is then calculated from the response time $\tau_{\hat{v}}$ of the vibration velocity amplitude to reach ~ 63% using Eq. (14). Finally, C is determined using the definition of ω_n in Eq. (9), and α is calculated based on Eq. (6).

In the application for the PUPS, the model parameters listed in Table 1 were identified from a frequency sweep at a driving voltage amplitude of 10 V and the response to a step of the driving voltage amplitude from 9 V to 10 V. A second set of model parameters was identified when a force of approximately 0.25 N was applied laterally at the tip of the PUPS to enable the simulation of a load step.

3.2. Calculation of controller gains

The method of pole-zero cancellation [31,32] is applied to achieve a critically damped first-order closed-loop behavior of the vibration velocity amplitude and phase with response times of $\tau_{CL_{\hat{v}}}$ and τ_{CL_ϕ}, respectively.

Given Eqs. (12), (13), (17) and (19), the closed-loop transfer functions for the vibration velocity amplitude and phase are given by

$$G_{CL_{\hat{v}}} \approx \frac{(K_{p_{\hat{v}}} + \frac{K_{i_{\hat{v}}}}{s})(\frac{\alpha}{2\,L\,s+R})}{1 + (K_{p_{\hat{v}}} + \frac{K_{i_{\hat{v}}}}{s})(\frac{\alpha}{2\,L\,s+R})} \quad \text{and} \tag{27}$$

$$G_{CL_\phi} \approx \frac{(K_{p_\phi} + \frac{K_{i_\phi}}{s})(\frac{-2\,L}{2\,L\,s+R})}{1 + (K_{p_\phi} + \frac{K_{i_\phi}}{s})(\frac{-2\,L}{2\,L\,s+R})}. \tag{28}$$

Consequently, to place the zeros of $G_{CL_{\hat{v}}}$ and G_{CL_ϕ} onto the poles of $G_{p_{\hat{v}}}$ and G_{p_ϕ}, respectively, the gains for the integral terms must fulfill

$$K_{i_{\hat{v}}} = \frac{K_{p_{\hat{v}}}\,R}{2\,L} \quad \text{and} \tag{29}$$

$$K_{i_\phi} = \frac{K_{p_\phi}\,R}{2\,L}. \tag{30}$$

With these gains (27) and (28) reduce to

$$G_{CL_{\hat{v}}} \approx \frac{K_{p_{\hat{v}}}\,\alpha}{K_{p_{\hat{v}}}\,\alpha + 2\,L\,s} = \frac{\frac{K_{p_{\hat{v}}}\,\alpha}{2\,L}}{s + \frac{1}{\tau_{CL_{\hat{v}}}}}, \quad \text{and} \tag{31}$$

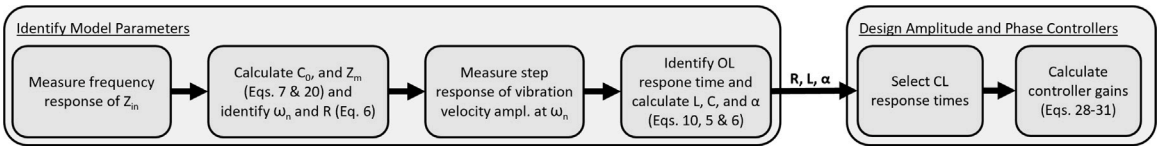

Fig. 3. Flow chart illustrating the parametric design of PI controllers with pole-zero cancellation for resonance frequency tracking and amplitude control of PUTs.

$$G_{CL_\phi} \approx \frac{K_{p_\phi}}{K_{p_\phi} - s} = \frac{-K_{p_\phi}}{s + \frac{1}{\tau_{CL_\phi}}}, \quad \text{with} \tag{32}$$

$$\tau_{CL_{\hat{v}}} = \frac{2\,L}{K_{p_{\hat{v}}}\,\alpha}, \quad \text{and} \tag{33}$$

$$\tau_{CL_\phi} = -\frac{1}{K_{p_\phi}}, \tag{34}$$

where $\tau_{CL_{\hat{v}}}$ and τ_{CL_ϕ} are the closed-loop response times of the amplitude and phase dynamics, respectively. Accordingly, the gains for the proportional terms must fulfill

$$K_{p_{\hat{v}}} = \frac{2\,L}{\alpha\,\tau_{CL_{\hat{v}}}} \quad \text{and} \tag{35}$$

$$K_{p_\phi} = -\frac{1}{\tau_{CL_\phi}} \tag{36}$$

to achieve the desired closed-loop response times. Thus, (29) and (30) can be rewritten as

$$K_{i_{\hat{v}}} = \frac{R}{\alpha\,\tau_{CL_{\hat{v}}}} \quad \text{and} \tag{37}$$

$$K_{i_\phi} = -\frac{R}{2\,L\,\tau_{CL_\phi}}. \tag{38}$$

For discrete-time controllers the gains to achieve pole-zero cancellation can correspondingly be calculated by

$$K_{p_{\hat{v}}} = \frac{R}{\alpha}\,\frac{e^{-\frac{T_s}{\tau_{CL_{\hat{v}}}}} - 1}{e^{-\frac{R\,T_s}{2\,L}} - 1}, \tag{39}$$

$$K_{p_\phi} = -\frac{R}{2\,L}\,\frac{e^{-\frac{T_s}{\tau_{CL_\phi}}} - 1}{e^{-\frac{R\,T_s}{2\,L}} - 1}, \tag{40}$$

$$K_{i_{\hat{v}}} = \frac{R}{\alpha\,T_s}\,(1 - e^{-\frac{T_s}{\tau_{CL_{\hat{v}}}}}), \quad \text{and} \tag{41}$$

$$K_{i_\phi} = -\frac{R}{2\,L\,T_s}\,(1 - e^{-\frac{T_s}{\tau_{CL_\phi}}}). \tag{42}$$

In the application for the PUPS, the target closed-loop response times were exemplarily chosen as $\tau_{CL_{\hat{v}}} = 1\,\text{ms}$ and $\tau_{CL_\phi} = 1\,\text{ms}$ and the gains of the two discrete-time PI controllers were calculated based on the model parameters of the unloaded PUPS listed in Table 1. This resulted in $K_{p_{\hat{v}}} \approx 34$, $K_{i_{\hat{v}}} \approx 3873$, $K_{p_\phi} \approx -810$, and $K_{i_\phi} \approx -92317$.

4. Experimental application

Fig. 4 depicts step responses measured on the PUPS in open-loop and in closed-loop with the PZC controllers, as well as corresponding simulations of the BVD model. In more detail, Fig. 4(a) depicts the responses to a step of the target vibration velocity amplitude from about 1.3 m/s to 2.3 m/s. In open-loop, the vibration velocity amplitude increased with a response time of approximately 8.5 ms in the measurement and the simulation. Simultaneously, the vibration velocity phase ϕ decreased from 20° to 0° in the measurements while it remained at 0° in the simulation. With the PZC PI controllers, the vibration velocity amplitude increased with a response time of 1 ms without overshoot, and the vibration velocity phase remained at 0°, as desired, in the measurement and the simulation. Fig. 4(b) depicts responses to a step of the target vibration velocity phase from 30° to 0°. In open-loop, the vibration velocity phase decreased with a response time of approximately 8.9 ms and 8.1 ms in the measurement and the simulation, respectively. Simultaneously, the vibration velocity amplitude increased from about 2 m/s to 2.3 m/s. With the PZC controllers, the closed-loop manifested the desired behavior again. The vibration velocity phase decreased to 0°, indicating that the system reached resonance, with a response time of approximately 1 ms and without undershoot, while the vibration velocity amplitude remained at approximately 2.3 m/s. Fig. 4(c) depicts responses to a step of the loading force from 0 mN to about 250 mN. In open-loop, the vibration velocity amplitude and phase substantially decreased in the measurement and the simulation due to the loading force. With the PZC controllers, the driving voltage amplitude gradually increased in reaction to the loading force while the driving frequency marginally decreased. Consequently, the vibration velocity amplitude and phase remained at approximately 2.3 m/s and 0°, respectively, in the measurement and the simulation.

Fig. 5 depicts step responses measured on the PUPS in open-loop and in closed-loop with the PZC controller in comparison to responses measured in closed-loop with PI controllers based on the other tuning methods presented in Section 2.8. Again, Fig. 5(a) depicts the response of the vibration velocity amplitude to a step of its target value from about 1.3 m/s to 2.3 m/s. With the PZC controller, the vibration velocity amplitude reached the new setpoint with a response time of about 1 ms without considerable overshoot, as mentioned previously. In contrast, the responses manifested a considerable overshoot with the controllers based on IMC and TL. The tuning methods ZN, MZN, KT14, and KT20, manifested even more prominent overshoots followed by subsequent oscillations. Responses of the vibration velocity phase to a step of the target phase from 30° to 0° are depicted in Fig. 5(b) and follow a similar pattern: The PZC controller showed the desired response time and no undershoot. With the controllers based on IMC and TL, a considerable undershoot resulted. An even higher undershoot and subsequent oscillations are visible with the other tuning methods. The vibration velocity amplitude measured during a step of the loading force from 0 mN to about 250 mN is shown in Fig. 5(c). All controller designs considerably reduced the distortion compared to the open-loop case. However, the PZC controller manifested the best load rejection and reduced the distortion of the vibration velocity amplitude to less than about 5.5%, as listed in Table 2.

5. Discussion

The results show that the proposed method to design the PI controllers for PUTs based on PZC can have several advantages in comparison to the other tested methods: The PZC controllers resulted in the best load rejection and in step-responses of the vibration velocity amplitude and phase without over- or undershoot and with a desired response time. Moreover, the PZC controllers can be designed based on a single risk-free experiment, and the entire design procedure can be automated.

Compared to the PZC method, all other tested tuning methods manifested an inferior load rejection, resulting in a higher distortion of the vibration velocity amplitude during a change of the loading force. The controller based on PZC reduced such distortions to less than about 5.5%. The controllers tuned using KT14, KT20, MZN, and TL exhibited inferior but acceptable load rejection, reducing the distortion to less than 10%. The controllers tuned using ZN and IMC resulted in high distortions during the load transient.

Furthermore, the step responses of the vibration velocity amplitude and phase measured on the PUPS during steps of the corresponding

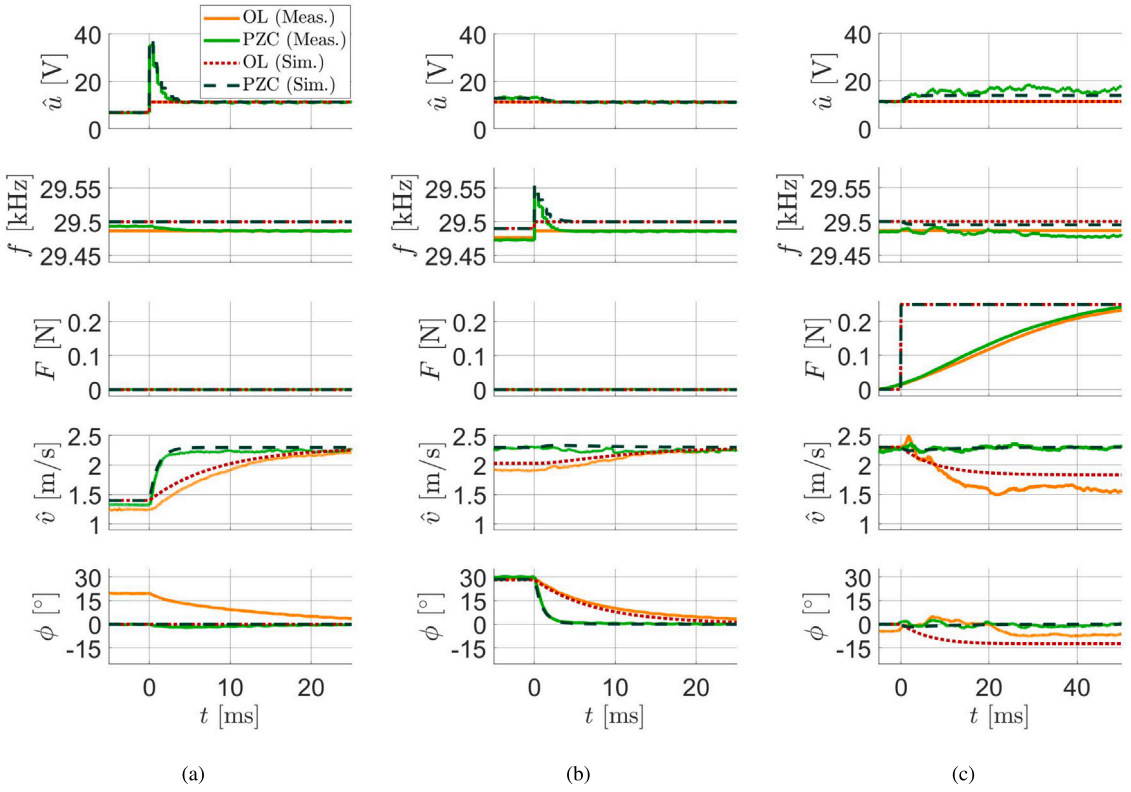

Fig. 4. Step responses measured (Meas.) on the piezoelectric ultrasonic periodontal scaler (PUPS) and corresponding simulations (Sim.) in open-loop (OL) and in closed-loop with the PI controller based on pole-zero cancellation (PZC). (a) Step of the target vibration velocity amplitude. (b) Step of the target vibration velocity phase. (c) Step of the loading force acting on the tip of the PUPS.

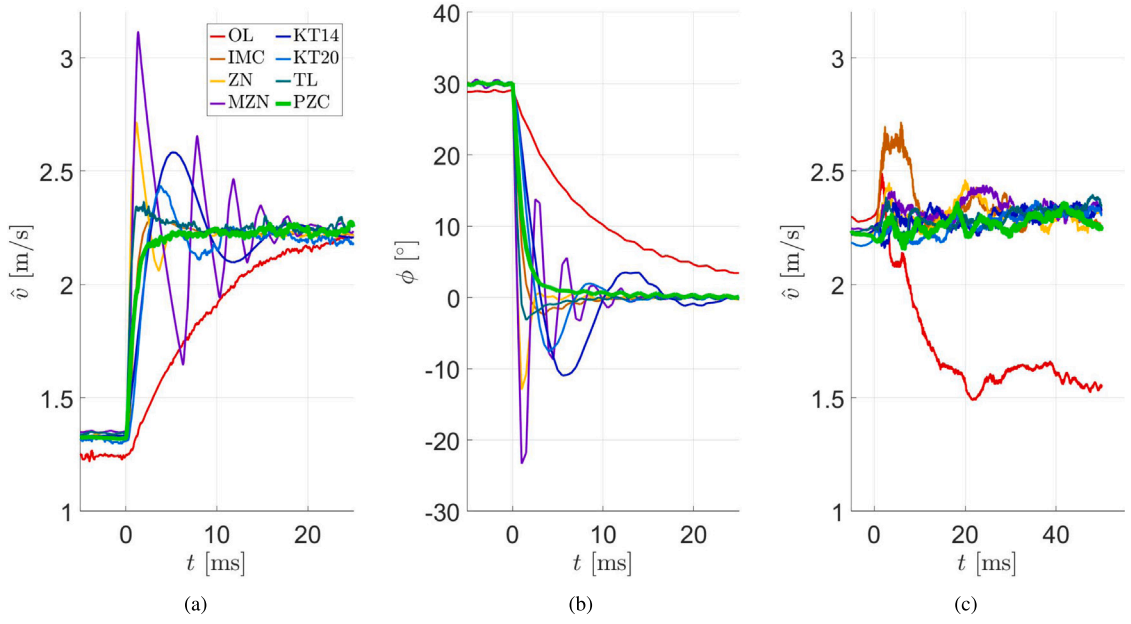

Fig. 5. Step responses measured on the piezoelectric ultrasonic periodontal scaler in open-loop (OL) and in closed-loop with PI controllers tuned using the internal model control (IMC), Ziegler–Nichols (ZN), modified Ziegler–Nichols (MZN), Kappa-Tau with $M_s = 1.4$ (KT14) and $M_s = 2.0$ (KT20), Tyreus-Luyben (TL), and pole-zero cancellation (PZC) method. (a) Step of the target vibration velocity amplitude. (b) Step of the target vibration velocity phase. (c) Step of the loading force acting on the tip of the PUPS.

setpoints manifested no over- or undershoot and the desired response time. In contrast, these step responses manifested a considerable over- and undershoot, respectively, when the controllers based on the other tuning methods were used. With the controllers based on the ZN, MZN, and KT methods, the step responses even manifested several oscillations.

As outlined in Section 3.1, two experiments were used to identify the model parameters of the PUPS for the application of the PZC and the IMC method. Alternatively, these model parameters can also be identified solely from the frequency response [1,6]. However, some effects, i.e., an influence of the driving voltage amplitude on a PUT's characteristics, are not captured by a frequency response. In this case,

Table 2
Characteristics of the responses of $\hat{v}$ to a step of $\hat{v}_{set}$, of ϕ to a step of ϕ_{set}, and of $\hat{v}$ to a step of the loading force in open-loop and in closed-loop with various PI controllers.

	$\hat{v}$ in Fig. 5(a)		ϕ in Fig. 5(b)		$\hat{v}$ in Fig. 5(c)
	Response-time[a]	Settling-time[b]	Response-time[a]	Settling-time[b]	Max. distortion[c]
Measured Open-Loop Response	8.5 ms	16.2 ms	8.9 ms	35.3 ms	35.1 %
Measured Closed-Loop Response with IMC	1.0 ms	1.5 ms	0.8 ms	1.4 ms	22.3 %
Measured Closed-Loop Response with ZN	0.4 ms	4.2 ms	0.3 ms	2.1 ms	10.9 %
Measured Closed-Loop Response with KT20	1.7 ms	39.7 ms	1.6 ms	6.0 ms	8.5 %
Measured Closed-Loop Response with MZN	0.6 ms	14.9 ms	0.3 ms	7.6 ms	8.4 %
Measured Closed-Loop Response with TL	0.4 ms	2.5 ms	0.5 ms	1.6 ms	7.8 %
Measured Closed-Loop Response with KT14	1.7 ms	13.7 ms	1.9 ms	14.3 ms	6.6 %
Measured Closed-Loop Response with PZC	1.0 ms	1.9 ms	1.1 ms	2.5 ms	5.5 %

[a] Time to reach 63.21% of the step height.
[b] Time to settle to a tolerance band of ±10% of the step height around the new setpoint.
[c] Maximum distortion in percent of the setpoint.

the method presented in Section 3.1 can lead to parameters more accurately reflecting the PUT's characteristics relevant to a control system. Additionally, the response times of the vibration velocity amplitude and phase may marginally differ, as visible in Table 2. It may thus be advantageous to identify different sets of model parameters based on the amplitude and phase step responses to design the corresponding controllers. However, if the difference is small, as in the present application, this is unnecessary, as can be seen in Table 2.

However, by means of simulations, we found that the performance of the PI controllers tuned with PZC is rather not sensitive to model parameter variations. If the equivalent circuit's resistance is overestimated by a factor of two, the step responses manifest an overshoot of only approximately ten percent, for instance. The results of this theoretical analysis are supported by practical experiments in which periodontal hygienists used the PUPS to remove artificial calculus. In this application, the characteristics of the PUPS can change considerably due to the varying operating conditions [1]. However, the closed system consistently performed as expected during these tests, with no noticeable alteration of the step responses or any sign of instability.

In contrast, an a priori unknown number of iterative experiments is required to parameterize the controllers using the ZN, MZN, KT, and TL methods. In the application for the PUPS, 27 experiments were required to design the controllers using these methods. Furthermore, the experiments to determine the ultimate gain and oscillation period, particularly of the amplitude controller, could be destructive for some PUTs. As an alternative, the so-called Relay Autotuning technique could potentially be used to estimate the ultimate gain and the corresponding oscillation period. However, modifications of the control system's hardware or software are required to enable such experiments. Further investigations would be required to study the impact of this technique for parameter estimation on the performance of controllers for PUTs, which was beyond the scope of this study.

While the high similarity of the measured and simulated responses depicted in Fig. 4 illustrates that the BVD model accurately mimics the behavior of the PUPS, the BVD model may not be valid to represent particular PUTs. The static BVD model does not reproduce effects that can influence the behavior of PUTs, i.e., drift, saturation, hysteresis, or influence of operating conditions. However, these limitations may be overcome by using extended versions of the BVD model [1–5]. In the case of the PUPS used in the present work, the most notable effect not reproduced by the BVD model is the influence of load on the transducer's characteristics, noticeable, e.g., in Fig. 4(c). In the simulations, the influence of load can be approximated by changing the values of the BVD model parameters as outlined in Section 2.7. Additionally, the driving voltage amplitude influences the resonance frequency of the PUPS, e.g., visible in Fig. 4(a). However, since this effect is comparatively small, the simulations correspond well with the responses measured on the PUPS, confirming the BVD model's validity in the present application.

As documented in previous work [6], the harmonic averaging model in Section 2.3 accurately reproduces the amplitude and phase dynamics of the BVD model, if $C/L \approx 0$ and if the driving frequency is close to the resonance frequency. In the case of the PUPS, $C/L < 10^{-10}$ and proximity to resonance is maintained in the closed-loop system by the feedback control, as can be seen in Figs. 4 and 5.

In some applications of PUTs, other types of controllers may be favorable. Pole-placement controllers, for instance, may improve load rejection compared to PI or PID controllers [31,32]. However, PI and PID controllers are widely used to control PUTs, as outlined in the introduction, since they can be implemented by analog or digital electronic systems with comparatively low complexity and still provide high performance. Purely proportional controllers may be sufficient in applications where offset-free tracking is not required [7,31]. However, in many applications of PUTs, offset-free tracking of the resonance frequency as well as the vibration velocity amplitude is crucial, requiring an integral action [7,31]. Conversely, extending the controllers with a differential term does not seem expedient in the given application. Adding a differential term would increase the complexity of the control system and the sensitivity to distortions. Moreover, since PUTs' amplitude and phase dynamics may be approximated by first-order transfer functions, as outlined in Section 2.3, a differential term is not required to stabilize the system or to achieve desired closed-loop response times. Furthermore, it should be noted that various other tuning methods for PI controllers other than those tested in the scope of this article and variations of the presented methods are described in scientific literature. Some of these methods may perform similarly to the proposed PZC method in some applications. However, based on the available results, PZC should, at least, be considered as an efficient tuning method to achieve high-performance controllers for PUTs.

Independent of the control algorithm, the electronic system used to implement the feedback controllers heavily influences the overall system's performance. High measurement noise may cause the driving voltage amplitude or frequency to exceed the system's output range, particularly if small closed-loop response times have to be achieved. Thus, great care should be taken to optimize the quality of measurements in similar applications.

The closed-loop transfer functions in Eqs. (27) and (28) suggest that arbitrary closed-loop response times can be achieved. Yet, smaller target response times entail larger variations of the driving voltage amplitude and frequency that may exceed the electronic system's output range. Moreover, it is generally advisable to select closed-loop response times at least 5 to 10 times greater than the sampling period of discrete-time feedback controllers. However, the electronic control system's small measurement noise and large output range facilitated to achieve closed-loop response times of 1 ms in the present application.

6. Conclusion

In this article, we presented a new method to identify model parameters and to parametrically design PI controllers for PUTs that track the resonance frequency and regulate the vibration velocity amplitude with high performance.

The parametric method to design PI controllers for PUTs based on pole-zero cancellation was experimentally applied to a PUPS and compared to other tuning methods. The proposed method required thirteen times fewer experiments than the Ziegler–Nichols method, for instance, and resulted in a system that manifested superior closed-loop behavior than any of the other tuning methods.

The present work can considerably facilitate and accelerate the design of highly effective feedback controllers for PUTs in various applications.

CRediT authorship contribution statement

Diego Stutzer: Writing – review & editing, Writing – original draft, Visualization, Validation, Software, Methodology, Investigation, Formal analysis, Data curation, Conceptualization. **André Lisibach:** Writing – review & editing, Validation, Formal analysis. **Martin Hofmann:** Writing – review & editing. **Jürgen Burger:** Writing – review & editing, Supervision, Funding acquisition. **Thomas Niederhauser:** Writing – review & editing, Supervision, Funding acquisition.

Declaration of competing interest

The authors declare that they have no known competing financial interests or personal relationships that could have appeared to influence the work reported in this paper.

Acknowledgments

This work was supported by the Swiss Innovation Agency Innosuisse, Switzerland (Project Grant Nr. 34901.1 IP-LS). The authors would like to thank Electro Medical Systems SA, Nyon, for providing the piezoelectric ultrasonic periodontal scaler that was used in this study.

Data availability

Data will be made available on request.

References

[1] Stutzer D, Hofmann M, Wenger D, Harmouch K, Lenoir D, Burger J, et al. Characterization and modeling of a planar ultrasonic piezoelectric transducer for periodontal scalers. Sensors Actuators A: Phys 2023;351(114131). http://dx.doi.org/10.1016/j.sna.2022.114131.

[2] Sutliff RW. The effects of loading on equivalent electric circuit models for piezoelectric transducers [dissertation], Miami University; 2018.

[3] Shuyu L. Load characteristics of high power sandwich piezoelectric ultrasonic transducers. Ultrasonics 2005;43(5):365–73. http://dx.doi.org/10.1016/j.ultras.2004.07.008.

[4] Ying C, Zhaoying Z, Gang-hua Z. Effects of different tissue loads on high power ultrasonic surgery scalpel. Ultrasound Med Biol 2006;32(3):415–20. http://dx.doi.org/10.1016/j.ultrasmedbio.2005.12.012.

[5] Duan C, Singh R. Dynamic analysis of preload nonlinearity in a mechanical oscillator. J Sound Vib 2007;301(3–5):963–78. http://dx.doi.org/10.1016/j.jsv.2006.10.042.

[6] Stutzer D. Robust feedback control of piezoelectric dental scalers [Ph.D. thesis], Bern, Switzerland: Graduate School for Cellular and Biomedical Sciences, University of Bern; 2024.

[7] Takasaki M, Maruyama Y, Mizuno T. Resonance frequency tracing system for langevin type ultrasonic transducers. In: International conference on mechatronics and automation. 2007, p. 3817–22. http://dx.doi.org/10.1109/ICMA.2007.4304183.

[8] Shi J, Liu B. Optimum efficiency control of traveling-wave ultrasonic motor system. IEEE Trans Ind Electron 2011;58(10):4822–9. http://dx.doi.org/10.1109/TIE.2011.2114316.

[9] Liu X, Colli-Menchi AI, Gilbert JGR, Friedrichs DA, Malang K, Sanchez-Sinencio E. An automatic resonance tracking scheme with maximum power transfer for piezoelectric transducers. IEEE Trans Ind Electron 2015;62:7136–45. http://dx.doi.org/10.1109/TIE.2015.2436874.

[10] Mu S, Tanaka K, Wakasa Y, Akashi T, Nishimura Y, Oka M. Intelligent IMC-PID control for ultrasonic motor. In: 2009 ICCAS-SICE. 2009, p. 1911–5. http://dx.doi.org/10.1109/ICNSC.2009.4919272.

[11] Ghenna S, Giraud F, Giraud-Audine C, Amberg M. Vector control of piezoelectric transducers and ultrasonic actuators. IEEE Trans Ind Electron 2018;65(6):4880–8. http://dx.doi.org/10.1109/TIE.2017.2784350.

[12] Kuang Y, Jin Y, Cochran S, Huang Z. Resonance tracking and vibration stablilization for high power ultrasonic transducers. Ultrasonics 2014;54(1):187–94. http://dx.doi.org/10.1016/j.ultras.2013.07.001.

[13] Furuya SI, Maruhashi T, Izuno Y, Nakaoka M. Load-adaptive frequency tracking control implementation of two-phase resonant inverter for ultrasonic motor. IEEE Trans Power Electron 1992;7(3):542–50. http://dx.doi.org/10.1109/63.145142.

[14] Yan G. High accuracy tracking of ultrasonic motor based on PID operation of sliding surface plus inverse system compensation. Sci Rep 2022;12(1):6829. http://dx.doi.org/10.1038/s41598-022-10632-y.

[15] Du P, Liu Y, Chen W, Zhang S, Deng J. Fast and precise control for the vibration amplitude of an ultrasonic transducer based on fuzzy PID control. IEEE Trans Ultrason Ferroelectr Freq Control 2021;68(8):2766–74. http://dx.doi.org/10.1109/TUFFC.2021.3078663.

[16] Mu S, Shibata S, Yamamoto T, Tanaka K, Nakashima S, Liu TK. Experimental study on speed control of ultrasonic motor using intelligent IMC-PID control. In: 2019 international conference on technologies and applications of artificial intelligence. 2019, p. 1–6. http://dx.doi.org/10.1109/TAAI48200.2019.8959888.

[17] Wang F, Shi B, Huo Z, Tian Y, Zhang D. Control and dynamic releasing method of a piezoelectric actuated microgripper. Precis Eng 2021;68:1–9. http://dx.doi.org/10.1016/j.precisioneng.2020.10.014.

[18] Liang W, Huang S, Chen S, Tan KK. Precision motion control of a linear piezoelectric ultrasonic motor stage. In: 2013 IEEE/ASME international conference on advanced intelligent mechatronics. 2013, p. 164–9. http://dx.doi.org/10.1109/AIM.2013.6584086.

[19] Wang F, Shi B, Huo Z, Tian Y, Zhao X, Zhang D. Smooth displacement/force switching control of a piezoelectric actuated microgripper for micro manipulation. In: 2019 IEEE international conference on manipulation, manufacturing and measurement on the nanoscale. 2019, p. 216–9. http://dx.doi.org/10.1109/3M-NANO46308.2019.8947404.

[20] Gao J, Caliskan H, Altintas Y. Sensorless control of a three-degree-of-freedom ultrasonic vibration tool holder. Precis Eng 2019;58:47–56.

[21] Youssef A. Optimized PID tracking controller for piezoelectric hysteretic actuator model. World J Model Simul 2013;9(3):223–34.

[22] Liang C, Wang F, Tian Y, Zhao X, Zhang D. Development of a high speed and precision wire clamp with both position and force regulations. Robot Comput-Integr Manuf 2017;44:208–17. http://dx.doi.org/10.1016/j.rcim.2016.09.006.

[23] Ziegler JG, Nichols NB. Optimum settings for automatic controllers. Trans Am Soc Mech Eng 1942;64(8):759–65. http://dx.doi.org/10.1115/1.2899060.

[24] Åström KJ, Hägglund T. PID controllers: theory, design, and tuning. Instrument Society of America; 1995, pp. 140ff and 206ff.

[25] Hassan AA, Al-Shamaa NK, Abdalla KK. Comparative study for DC motor speed control using PID controller. Int J Eng Technol 2017;9:4181–92.

[26] Rivera DE, Morari M, Skogestad S. Internal model control. 4. PID controller design. Ind Eng Chem Process Des Dev 1986;25:252–65.

[27] Ille I, Twiefel J. Model-based feedback control of an ultrasonic transducer for ultrasonic assisted turning using a novel digital controller. Phys Procedia 2015;70:63–7. http://dx.doi.org/10.1016/j.phpro.2015.08.043.

[28] Berto LA, Ettmayer J, Stutzer D, Nietzsche S, Spiezia G, Niederhauser T, et al. In-vitro effects of novel periodontal scalers with a planar ultrasonic piezoelectric transducer on periodontal biofilm removal, dentine surface roughness, and periodontal ligament fibroblasts adhesion. In: Clinical oral investigations. 2024.

[29] Hofmann M, Stutzer D, Nassisi Q, Niederhauser T, Harmouch K, Spiezia G, et al. New approaches of planar piezoelectric ultrasonic transducers for effective periodontal scaling and care. In: Proceedings of ultrasonic industry associaction symposium.

[30] Stutzer D, Hofmann M, Eick S, Scharp N, Burger J, Niederhauser T. In vitro measurement of forces during debridement with a piezoelectric ultrasonic periodontal scaler, oral health and preventive dentistry. 2024.

[31] Doebelin E. Control system principles and design. Ernest Otto Doebelin; 1985.

[32] Sajnekar DM, Deshpande SB, Moharil RM. Comparison of pole placement & pole zero cancellation method for tuning PID controller of a digital excitation control system. Int J Sci Res Publ 2013;(4):358–65.

[33] Ieee standards board. In: IEEE standard on piezoelectricity. IEEE; 1996.

[34] Franklin GF, Powell JD, Emami-Naeini A. Feedback control of dynamic systems. Pearson; 2015, pp. 144 and 611-626.

[35] Wenger D. Implementation and verifcation of a modular platform to test controllers for piezoelectric ultrasonic periodontal scalers [Master thesis], Biel, Switzerland: Institute for Human Centered Engineering, Bern University of Applied Sciences; 2023.

Diego Stutzer earned the M.Sc. degree in electrical engineering and information technology at the Swiss Federal Institute of Technology Zürich (ETHZ) in 2007 with a specialization in biomedical technology. Subsequently he worked in various companies on industrial and research projects as a development engineer and head of engineering. Currently he is studying for a Ph.D. at the Graduate School for Cellular and Biomedical Sciences of the University of Bern and the Bern University of Applied Sciences.

André Lisibach did an Apprenticeship as a mechanic at Andritz Hydro. After obtaining his B.Sc. degree in Mechanical Engineering at Lucerne University of Applied Sciences, specializing in hydraulic machinery, he obtained an M.Sc. degree in Theoretical Physics from ETH Zurich. Subsequently, he worked in the field of computational fluid dynamics at Lucerne University of Applied Sciences in collaboration with the Swiss Center for Electronics and Microtechnology. He obtained his Ph.D. degree in mathematical physics at ETH Zurich, specializing in partial differential equations of gas dynamics. He is currently a Professor for mathematics at the Bern University of Applied Sciences (BFH). Before joining BFH he was an Associate Research Scholar at the Department of Mathematics at Princeton University, where he was working on the description of shock waves in gas dynamics.

Martin Hofmann completed an apprenticeship as an automation technician in 2012 and graduated from the Zurich University of Applied Science with a bachelor's degree in systems engineering in 2016. Martin Hofmann earned this M.Sc. degree in biomedical engineering at the University of Bern and the Bern University of Applied Sciences in 2018 and worked at the University of Applied Sciences Western Switzerland. He obtained his Ph.D. in Biomedical Engineering at the University of Bern in 2023 and currently works as a research associate at the School of Biomedical and Precision Engineering at the University of Bern.

Jürgen Burger is full professor for Translational Medicine and Precision Engineering at the Faculty of Science and Faculty of Medicine of the University of Bern. He is also Director at the School of Biomedical and Precision Engineering. His professional experience includes employment at Centre Suisse d'Electronique et de Microtechnique CSEM, Tegimenta AG (a Hoffmann-La Roche company), and Head of R&D Microsystems at Codman, a Johnson and Johnson company. After a research stay at Swinburne University, Melbourne, Australia, in 2003 and various appointments to professorships in Biomedical Engineering, including Charité, Humboldt-University, Berlin, University of Sydney, and University of Stuttgart, he obtained his Habilitation in 2008 at the University of Bern in "Biomedical Engineering" where he was appointed associate Professor (Titularprofessor) in 2014. Jürgen Burger's research focuses on bringing innovative treatment methods and therapeutic/diagnostic systems into clinical application. A special focus is on intelligent implants and surgical instruments in combination with pharmaceutical products.

Thomas Niederhauser earned his Master's and Ph.D. degree in biomedical engineering at the University of Bern. Subsequently, he worked as a research associate and lecturer at the University Hospital of Bern (Inselspital), and the Bern University of Applied Sciences. In 2018, he was appointed professor for biomedical signal processing and control and is currently also the head of the Institute for Human Centered Engineering at the Bern University of Applied Sciences.